Morphology Development via Reaction-Induced Phase Separation in Flexible Polyurethane Foam

Wu Li and Anthony J. Ryan*

Department of Chemistry, University of Sheffield, Sheffield S3 7HF, UK

Ingrid K. Meier

Air Products and Chemicals, Inc., 7201 Hamilton Boulevard, Allentown, Pennsylvania 18195-1501

Received January 8, 2002; Revised Manuscript Received April 2, 2002

ABSTRACT: Morphology development during reaction-induced phase separation in flexible polyurethane (PU) foam has been studied by time-resolved, small-angle X-ray scattering. Two different PU foaming systems, based on industrial formulations, have been studied. The scattering data have been analyzed using the Cahn−Hilliard model and fit to a Teubner−Strey microemulsion structure factor to extract morphological characteristics. Microphase separation was observed to follow spinodal decomposition kinetics; a bicontinuous morphology developed and was subsequently preserved by vitrification of the urea domains. The data analysis demonstrated that the amphiphilicity factor increases as the reactions proceed, due to the continuous formation of block copolymer poly(ether−urea).

Introduction

Reaction-induced phase separation (RIPS) generally proceeds from an initially homogeneous solution via liquid−liquid phase separation to yield a regular phase-separated morphology in the course of reaction. It is caused by the molecular weight increase of the polymer and by the variations of the interaction with conversion as a result of the accompanying chemical modifications. These collective changes may cause the system to cross thermodynamic phase boundaries and result in a transition from an initial homogeneous state into a microphase-separated state. RIPS occurs in a number of multiphase systems such as polyurethane,[1−3] rubber-modified epoxies,[4] and thermoplastics/thermoset alloys.[5−7] The final morphology of the resulting polymer is strongly dependent on the kinetic competition between phase separation rates and reaction rates and the connectivity between the phases. Several two-phase structures, (i.e., co-continuous structures, uniform spherical domain structures, and bimodal spherical domain structures) have been accessed via RIPS through the control of the relative rates of reaction and phase separation.[5]

Water-blown flexible polyurethane foam is made by simultaneous chemical reactions between a diisocyanate and both polyether polyol and water. Combination of these two exothermic reactions results in the formation of a multiblock copoly(urethane−urea) of the $-(H_mS)_n-$ type. The carbon dioxide gas evolved from the water−isocyanate reaction blows the polymer into a foam. Because the center of the foam bun is self-insulated by the surrounding polymer, the foaming process occurs under quasi-adiabatic conditions. The development of morphology during foaming is complex. As the chemical reactions proceed, the urea chain length increases and the interaction between the polyether soft and polyurea hard segments also changes. Such changes lead to a transition from an initial homogeneous state to a microphase-separated state at a critical conversion of isocyanate groups. The microphase-separated hard segments continue to grow, and association of the urea hard segments occurs. At the same time, strong hydrogen bonds between the urea groups can be formed within the hard domains; microphase separation is intercepted and quickly arrested by vitrification of the phase that is richer in hard segments. In summary, with branched reactants, a combination of chemical cross-linking, reaction-induced microphase separation, hydrogen-bond formation, and vitrification occurs during the foaming process. Therefore, the resultant morphology will reflect all these phenomena and is determined, in part, by the kinetic competition between these processes. It has been observed that the changes in the concentration of catalyst, cross-linker, and water strongly affect the foam morphology development and the resulting mechanical properties.[8,9]

FTIR spectroscopy has been employed to investigate both the reaction kinetics and the development of polymer structure during foam formation.[10−13] Hydrogen-bonding studies can often provide information concerning the phase separation of polyurea chains. Onset of microphase separation of soluble urea hard-segment sequences in slabstock foam was observed to occur after 50−60% of the isocyanate functional groups had been reacted. As the amount of water and/or catalyst increased in the formulation, the time to hard domain formation decreased. However, IR spectroscopy can only provide information concerning the microphase separation of polyurea chains for foams with well-ordered hydrogen bonds; furthermore, it cannot discern the mechanism by which microphase separation occurs.

The significance of the polyurea phase separation in relation to the rise in polymer modulus and foam stability after cell opening has been studied by rheometry.[8,14−16] It was observed that the storage modulus starts to increase at the onset of microphase separation of the urea hard segments. The modulus buildup in the foam arises from the growth of the physical network of hydrogen-bonded urea hard segments. The domains act as the "physical cross-links" and reinforcing filler.

SAXS has also been used to investigate the phase separation kinetics during the foaming process.[12,17]

10.1021/ma020035e CCC: $22.00
Published on Web 06/11/2002

Table 1. Details of Polyurethane Foam Formulations

reagent	description	TDI foam (pphp)	MDI foam (pphp)
Hyperlite E824	polyether polyol	74	
Hyperlite E852	polyether polyol	26	
Voranol V232-027	polyether polyol		100
Voranol CP 1421	polyether polyol		1.5
DABCO DC5043	silicone surfactant	0.75	
DABCO DC5169	silicone surfactant	0.25	
DABCO DC2585	silicone surfactant		0.40
DABCO BL11	amine catalyst	0.08	0.32
DABCO 33LV	amine catalyst	0.30	0.13
water	deionized (in-house)	3.5	3.5
diethanolamine	technical grade	1.49	0.6
Voranate T-80	isocyanate	105 index	
Mondur MRS-5	isocyanate		100 index

Elwell and co-workers [12,17] carried out dynamic IR and SAXS experiments on methylene diphenyl diisocyanate (MDI) foam formulations. There was a close agreement with the onset of microphase separation detected by FTIR spectroscopy and SAXS. The scattering data were also analyzed using a time-dependent Ginzburg−Landau model (TDGL) and yielded results that were in qualitative agreement with the theoretical predictions of the TDGL model and fit Cahn−Hilliard theory. It was concluded that microphase separation of urea hard segments during the formation of flexible polyurethane foam proceeds via spinodal decomposition.

The final morphology of PU has been extensively studied using transmission electron microscopy (TEM) and SAXS[18−20] and recently atomic force microscopy (AFM).[21,22] Cooper[18] observed lamellar and cylindrical morphologies from TEM for a series of PU elastomers with semicrystalline hard segments. Using AFM, Mclean and Sauer[21] observed that symmetric hard segment domains fill space uniformly in a segmented PU, which differs from those of block copolymers with equilibrium structure.

The two most common polyurethane foams are a toluene diisocyanate (TDI)-based and an MDI-based foam system. TDI foam is possible at a range of densities and has better overall physical properties, while MDI foam is easier to achieve variable firmness and MDI is an easier material to handle. Typical formulation reactivities mean details of formulation have to change. For many formulations, the effects of catalyst concentration are to the reaction rate and foam cell size whereas surfactant only changes foam cell size. However, the morphology development sequence is expected to remain the same. In this paper, the morphology developments in a TDI-based and an MDI-based flexible high-resilience (HR) polyurethane foam system were observed in situ using synchrotron SAXS under forced-adiabatic conditions. That the phase separation kinetics apparently follow spinodal decomposition kinetics was confirmed for the two different chemical systems. The SAXS data were analyzed using the microemulsion model developed by Teubner and Strey,[23] and the amphiphilicity of the systems was quantified. The final morphology of PU foam was studied by atomic force microscopy (AFM).

Experimental Section

Materials. Representative TDI-based and MDI-based HR foam formulations, both with a total water concentration of 3.5 g per 100 g of polyol, were employed. Formulation details are listed in Table 1. In the following discussion, the TDI-based formulation will be referred to as "TDI foam" and the MDI-based formulation will be referred to as "MDI foam". Isocyanate Voranate T-80 (Dow Chemical Co.) is an 80:20 mixture of the 2,4- and 2,6-isomers of toluene diisocyanate. The polyol Hyperlite E824 (Arco Chemical) is nominally a triol containing 78% propylene oxide (PO) and 22% ethylene oxide (EO) with terminal primary hydroxyl groups. Hyperlite E852 (Arco Chemical) is a poly(styrene−acrylonitrile)-filled polyol containing 80% PO and 20% EO. Isocyanate Mondur MRS-5 is a 4,4′-MDI-rich polymeric MDI. Voranol V232-027 (Dow Chemical) is a triol containing 83% PO and 17% EO with terminal primary hydroxyl groups. Polyol Voranol CP 1421 is a polyol that has a very high EO content. The catalysts employed for both foaming systems were tertiary amine catalysts DABCO 33LV, 33% triethylenediamine in dipropylene glycol and BL11, 70% bis(2-dimethylaminoethyl) ether in dipropylene glycol (Air Products and Chemicals, Inc.), and the silicone surfactants were DABCO DC5043, DC5169, and DC2585 (Air Products and Chemicals, Inc.). All ingredients were used as received after standard characterization techniques were used to confirm their functionality.

Synchrotron SAXS. SAXS measurements were conducted on beamline 16.1 at the Synchrotron Radiation Source (SRS, CLRC Daresbury Laboratory, Warrington, UK) using 1.41 Å wavelength X-rays. A multiwire area RAPID detector was used at a sample distance of 3.5 m, and data were collected every 3 s over a period of 765 s. The temperature-controlled SAXS cell was similar to that used by Elwell.[17] It comprised two outer plates which were fit with thermocouples. The plates had counter-sunk holes of 6 mm in diameter which were covered with polyimide (Kapton) windows of 10 μm nominal thickness. A poly(tetrafluoroethylene) (PTFE) insert of 4 mm thickness formed the "mold". The SAXS cell was positioned between the exit window of the beamline and the entrance window of the vacuum chamber. The temperature of the sample cell was recorded and controlled by a 586 personal computer equipped with Strawberry Tree Datashuttle data acquisition hardware running a Workbench 3.00 software package. The temperature control program was designed so that the thermocouple readings matched prerecorded temperature profiles for the appropriate foam formulations.

The reactants were remotely mixed and injected into the SAXS cell by a static mixer apparatus which consisted of a static mixer, disposable polypropylene syringes, and pneumatic cylinders. The polyol, surfactant, catalyst, cross-linker, and water were premixed using a mechanical mixer before transferring the resultant "premix" to a syringe. The syringe containing the polyol premix and one containing the isocyanate were emptied pneumatically, under a drive pressure of 80 psi, by two drive cylinders linked through a fixed cross arm, in a device which could be activated remotely. A disposable static mixer, fit with a 32-element insert, was employed as the mix-head which was connected to the SAXS cell via PVC tubing (internal diameter of 3 mm). It took 3−5 s to fire all reactants into the sample cell. The schematic diagram that shows the complete experimental arrangement employed is illustrated in Figure 1.

The experimental SAXS data were recorded for three separated runs for each foaming system with a time resolution of 3 s and corrected for background scattering (subtraction of the scattering from the camera and the empty cell), sample thickness, and transmission. Then the two-dimensional data were transformed into one dimension by performing sector integration over an arc width of 60°. The reduced data were obtained in terms of intensity vs the scattering wave vector.

AFM Experiments. The experiments were performed on a Nanoscope IIIa AFM from Digital Instruments using tapping mode and phase imaging. Silicon Nitride probes with 125 μm long cantilevers were used at resonance frequencies which typically varied from 270 to 290 kHz. The AFM was operated in ambient with a double-vibration isolation system. The lateral scan frequency was about 1 Hz.[24] Small foam samples were embeded in epoxy which cured at 60 °C for 48 h. The cross sections were microtomed to smooth surface and then examined by AFM.

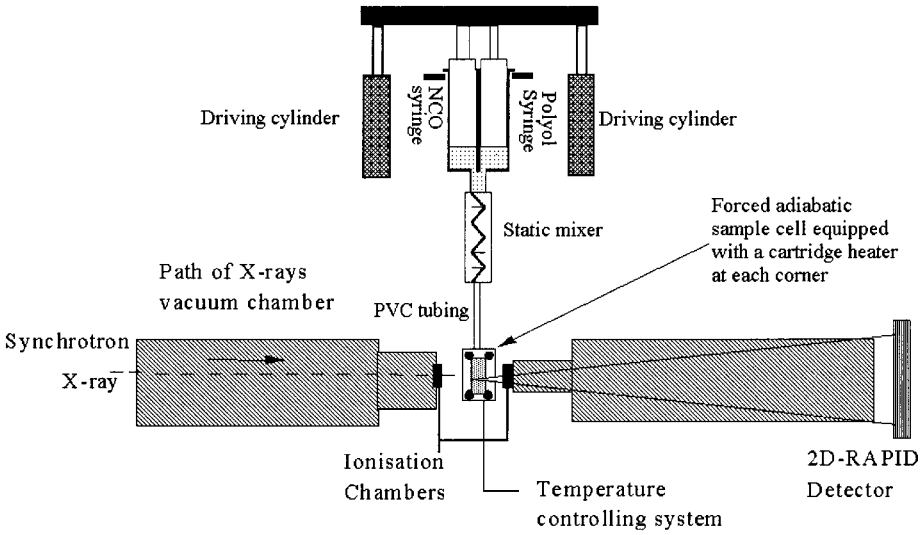

Figure 1. Schematic diagram illustrating the experimental arrangement within the X-ray hutch.

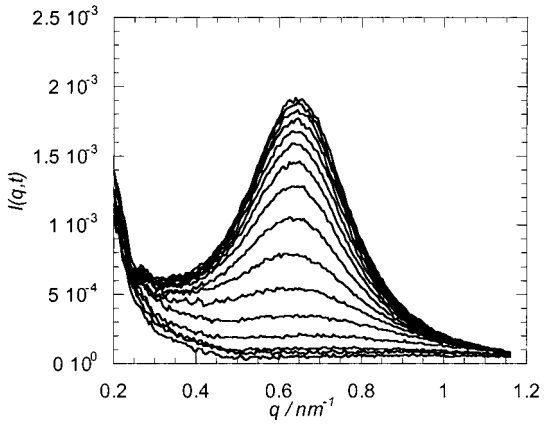

Figure 2. Plot of scattered intensity, $I(q,t)$, vs scattering vector q, at selected times for a representative data set of TDI foam. From the bottom going upward, the curves represent the SAXS pattern from reaction time 69 to 159 s every 6 s.

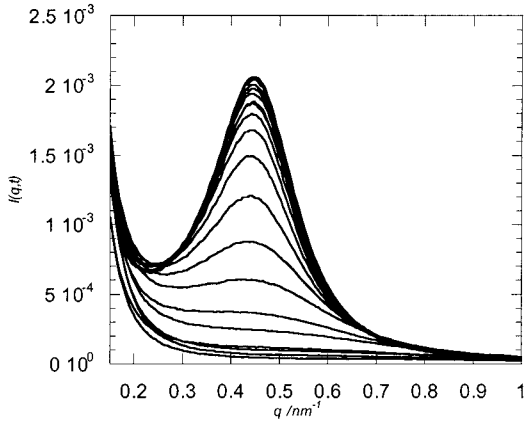

Figure 3. Plot of scattered intensity, $I(q,t)$, vs scattering vector q, at selected times for a representative data set of MDI foam. From the bottom going upward, the curves represent the SAXS pattern from reaction time 33 to 147 s every 6 s.

Results and Discussion

Synchrotron X-ray Scattering. Figures 2 and 3 show representative plots of scattered intensity $I(q,t)$ vs scattering vector q at selective times for TDI foam and MDI foam, respectively. In the scattering vector range studied, no scattering peak can be observed for either system in the early stage of the reaction. The liquid mixture which was injected into the cells comprises unreacted monomer, short urea hard segments, and isocyanate-tipped polyether oligomers; it is homogeneous (with the exception of some gas bubbles) at this stage. In the case of TDI foam, there is the first appearance, after 75 ± 3 s, of a scattering maximum at $q \approx 0.59$ nm^{-1}, which indicates the onset of microphase separation. The peak intensity increases rapidly until approximately 120 s, after which the growth of peak intensity slows and then becomes approximately constant. At this time, microphase separation is intercepted and quickly arrested by the vitrification of the phase that is richer in hard segments. This phase has attained a composition with a glass transition temperature T_g equal to that of the surrounding polymer medium.

A similar sequence of events is also observed in the MDI foam, where the scattering maximum occurs at $q \approx 0.47$ nm^{-1} after 45 ± 3 s. The intensity of this scattering maximum continuously and rapidly increases until approximately 100 s, at which point it slows down and becomes approximately constant after 150 s. Again, this occurs because the microphase separation is arrested by the vitrification of urea hard-segment domains. The MDI scattering data are less noisy than that of TDI foam, which is due to the higher electron density contrast between the hard- and soft-segment domains in MDI foam. For both foaming systems, the scattering peak is quite broad due to the large distribution of interdomain spacings.

The development of the total scattered intensity, or invariant Q, can be related to the onset of microphase separation during the foaming process. The invariant is independent of the size or spatial arrangement of the structural inhomogeneities and is expressed as[25]

$$Q = \int_0^\infty I(q)q^2\,\mathrm{d}q \sim \phi_1\phi_2(\rho_1 - \rho_2)^2 \qquad (1)$$

where ρ_i and ϕ_i are the electron density and volume fraction, respectively. The invariant can be employed to characterize the structure development as well as the degree of microphase separation: an increase in Q corresponds to an increase in the degree of phase separation. In this study, a relative invariant Q' is calculated from the relative intensity experimental data by summation of the area under the $I(q)q^2$ vs q curve

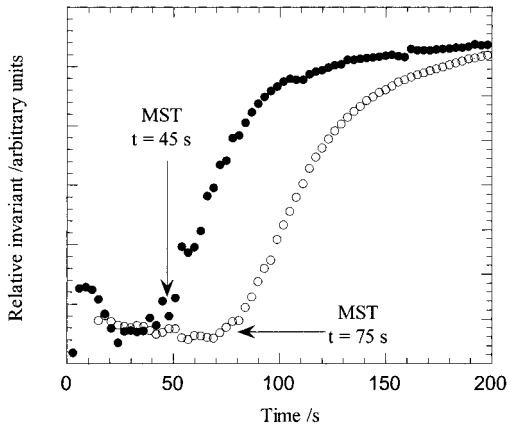

Figure 4. Plots of the relative invariant Q' as a function of time for TDI foam (○) and MDI foam (●).

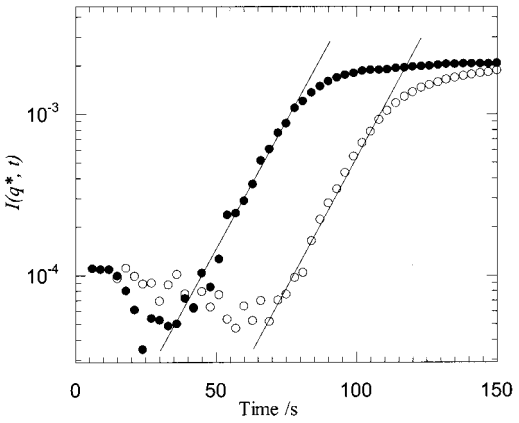

Figure 5. Plots of ln $I(q^*,t)$ as a function of time for TDI foam (○) and MDI foam (●).

between the first reliable data point at $q = 0.2$ nm^{-1} and the region where $I(q)q^2$ becomes dominated by the thermal noise at $q = 1.2$ nm^{-1}. The relative invariant represents the biggest contribution to the magnitude of Q and gives a quantitative indication of the growth in electron density fluctuations.

Figure 4 plots the relative invariant as a function of time for the TDI and MDI foams. The cause of the initial decrease in the relative invariant is thought to be due to the contribution to Q' from microvoid (bubble) scattering,[17] and as the bubbles grow larger (∼1 mm), they scatter less in this q range. The onset of microphase separation is taken as the point at which Q' starts to increase rapidly. The onset of microphase separation of TDI foam occurs at 75 ± 3 s, which corresponds to an isocyanate conversion P_{NCO} of 0.66 ± 0.02. The isocyanate conversion was obtained from normalized temperature rise profile using the adiabatic reactor method:

$$P_{NCO} = \frac{T_t - T_0}{r\Delta T_{ad.calc}} \tag{2}$$

where r is the isocyanate index, T_t is foam temperature at time t, T_0 is the initial temperature, and $\Delta T_{ad.calc}$ is the calculated adiabatic temperature rise.[9,26] When compared with the values of 50−60% isocyanate conversion for slabstock TDI foam,[8,13] the P_{NCO} of the TDI system described here is relatively high. We have found this to be due to the effect of the diethanolamine (DEOA) cross-linker on the microphase separation, and this will be dealt with in subsequent publications. For the MDI foam, the onset of phase separation is 45 ± 3 s. This corresponds to an isocyanate conversion P_{NCO} of 0.35 ± 0.02, which is much lower than that of conventional slabstock MDI foam. Although DEOA will also delay the onset of phase separation in MDI foams, the existence of the higher MDI oligomers, which are highly incompatible with the polyether soft segments, results in microphase separation at lower conversions. As the foaming reaction continues, the degree of polymerization of hard blocks, i.e., the quench depth, continues to increase. In phase separation in nonreactive binary blends, a quench is normally isothermal, and thus, the driving force for phase separation remains constant; i.e., there is an isoquench. In reactive mixtures, the quench depth increases continuously as the reaction progresses because the polymer molecular weight increases and the isoquench conditions are lost. Reactive polyurethanes violate the normal assumptions of phase separation in binary mixtures on two counts: first, they are not isoquenches, and second, the reaction generates additional components which can act as surfactants.

Depending upon the quench depth, the foaming mixture can phase separate by either nucleation and growth (NG) or spinodal decomposition (SD) mechanisms. The SD mechanism can lead to the formation of a nonequilibrium bicontinuous morphology at the beginning of microphase separation, whereas the NG mechanism leads to a continuous/dispersed phase morphology. For well-characterized NG systems, the scattered intensity should decrease monotonically with the scattering vector and increase with the square of time at a fixed angle. In the case of SD, the linearized theory of Cahn and Hilliard[27] predicts that the compositional fluctuations, and thus the scattered intensity, have a maximum for a given wavelength. If spinodal decomposition is the mechanism of microphase separation, then peak position q^* should remain constant in the early stages, but the peak intensity should exhibit an exponential increase with time as shown in eq 3:

$$I(q,t) = I(q,0)\exp[2R(q)t] \tag{3}$$

where $R(q)$ is the amplification rate of the composition fluctuations[28,29] and depends on q. Therefore, a plot of ln $I(q)$ vs t should give a straight line during the early stages of phase separation. $R(q)$ is described by

$$R(q) = -Mq^2\left(\frac{\partial^2 f}{\partial c^2} + 2\kappa q^2\right) \tag{4}$$

where M is a translational diffusion constant, f is the free energy density of a homogeneous system at composition c, and κ is an energy gradient coefficient.

The strong peak in the scattering profiles suggests that the phase separation occurs via spinodal decomposition. However, reaction-induced SD is different from isothermal decomposition. We were interested in testing whether the linearized theory could be applied to the early stage of the reaction-induced phase separation. Figure 5 illustrates representative plots of ln $I(q^*,t)$ vs time for TDI foam and MDI foam. It is apparent that there is a good fit of the ln $I(q^*,t)$ data to a straight line after the onset of microphase separation. The values of $R(q)$ are calculated from the slopes of the ln $I(q,t)$ vs t curves and taken as half of the value of the gradient. $R(q)$ is the rate at which the amplitude at q increases, and a linear relationship between $R(q)/q^2$ and q^2 is predicted from the theory of Cahn and Hilliard. The

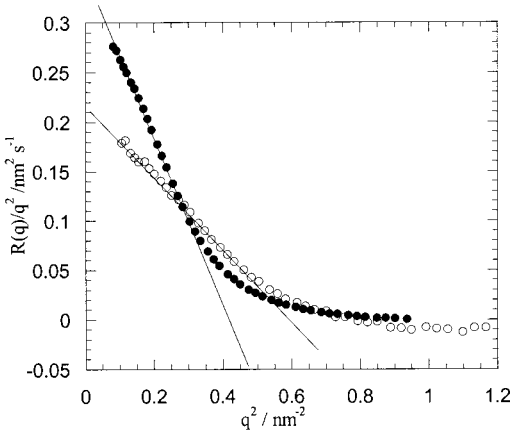

Figure 6. Plot of $R(q)/q^2$ vs q^2 for representative data sets obtained from TDI foam (○) and MDI foam (●).

values of $R(q)/q^2$ vs q^2 for TDI foam and MDI foam are plotted in Figure 6. The data are linear at low values of q, suggesting the validity of the linearized theory. A deviation from linearity is observed at larger q values. In isoquenches this behavior is attributed to the fact that the linearized theory neglects the random thermal force and, most importantly in this case, the reaction that is occurring during phase separation which continuously increases the quench depth.

The effective diffusion coefficient D_{eff} of polyether soft segments may be calculated from the extrapolation to $q = 0$ of the linear portion of $R(q)/q^2$:[30]

$$D_{\text{eff}} \underset{(q\to 0)}{=} -\frac{R(q)}{q^2} \tag{5}$$

The magnitude of D_{eff} is a measure of the ease with which the blocks diffuse and is a product of the quench depth and the relative mobility. The higher the value of D_{eff}, the less resistance the blocks encounter as microphase separation occurs. The negative diffusion coefficients indicate diffusion against the composition gradient (i.e., from a region of low concentration to a region of high concentration) as found in spinodal decomposition of a mixture.[27,31,32] The values of D_{eff} are -0.22 ± 0.02 and -0.35 ± 0.01 nm^2 s^{-1} for TDI foam and MDI foam, respectively. The negative effective diffusion coefficients strongly support the SD mechanism. The above analyses are based on the implicit assumptions that M, κ, and $f(c)$ are constant (being independent of time and composition). In general, these assumptions cannot be satisfied in these reactive systems. However, the good fit may suggest that either the assumptions are approximately true in the very early stage of the reaction-induced spinodal decomposition or that the coefficients vary in such a way as to cancel each other out. For example, the reaction causes an increase in molecular weight and thus decreases mobility, but it also causes the temperature to increase and thus increases mobility.

Theoretical studies[33,34] have shown that, under successive increases in quench depth, SD yields a regular two-phase structure resulting from SD under an isoquench. The kinetics of microemulsion formation via spinodal decomposition induced by a thermal quench in multicomponent polymer blends has been studied by experiments[30,35,36] and computer simulations.[37] Polymeric microemulsions are obtained by adding diblock copolymers, which have favorable enthalpic interactions with one or both of the homopolymer phases. These favorable thermodynamic interactions increase the driving force for interfacial segregation so that the interfacial tension can be driven to zero or to a slightly negative value. The interface becomes unstable, leading to spontaneous formation of a deeply corrugated interface with copolymer-coated droplets nearby. Similar to ternary polymer blends, at the onset of microphase separation the foaming systems comprise polyether, polyurea, and block copolymer polyether−polyurea formed by a urethane group. Thus, a microemulsion-like structure could also be formed in the foam via a spinodal decomposition mechanism. To study the development of this bicontinuous morphology via RIPS during foaming, the scattering data were analyzed using the Teubner and Strey model.[23] The same Ginzburg−Landau free energy expansion used to derive the SD model was used as a starting point for the derivation, by Teubner and Strey, of a scattering intensity function $I(q)$ (structure factor) for a three-component amphiphilic microemulsion,

$$I(q) = \frac{1}{a_2 + c_1 q^2 + c_2 q^4} \tag{6}$$

where a_2, c_1, and c_2 are composition-dependent coefficients and q is the magnitude of the scattering wave vector. Because the same free energy function is used in the analysis of the phase separation kinetics and the microemulsion structure factor, we used this structure factor to extract morphological information from the developing polyurethane foam. The Teubner−Strey model was first employed to analyze SAXS and SANS data for water/oil/surfactant (o/w/s) systems,[23,38] and it was later extended to polymer blend systems.[39,40]

It is essential to have the coefficient $c_1 < 0$, as well as $a_2 > 0$ and $c_2 > 0$, to obtain a peak in the scattering curve $I(q)$ at finite q. The model has led to two important characteristic lengths, D and ξ, which appear in the spatial correlation function of the system. While the length D is characteristic of the domain size (the periodicity) of the system, the correlation length ξ represents the length over which the structural correlation decays exponentially. From the values of the three coefficients a_2, c_1, and c_2, the domain size D can be calculated using eq 7:[23]

$$D = 2\pi\left[\frac{1}{2}\left(\sqrt{\frac{a_2}{c_2}} - \frac{c_1}{2c_2}\right)\right]^{-1/2} \tag{7}$$

Equation 8 can be used to calculate the correlation length ξ:

$$\xi = \left[\frac{1}{2}\left(\sqrt{\frac{a_2}{c_2}} + \frac{c_1}{2c_2}\right)\right]^{-1/2} \tag{8}$$

The experimental scattering data were fit to eq 6. The data for the TDI foam at three reaction times are shown in Figure 7. These times represent a point just after the onset of microphase separation, a point at which the scattering intensity leveled off, and a point long after the onset of microphase separation. The Teubner−Strey fits at each time are very good, indicating the presence of a microemulsion morphology in the foam. Previous results[41] suggest a bicontinuous morphology is preserved when the spinodal decomposition process is

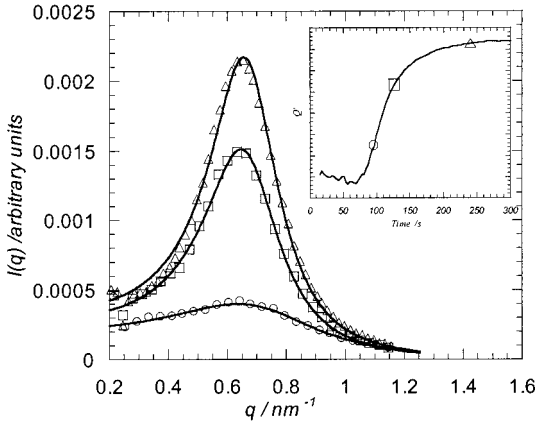

Figure 7. Scattering intensity $I(q)$ at selective time from TDI foam and fitted curves (from eq 6) in various lines as a function of q: (○) 96 s, (□) 126 s, (△) 240 s. The inset shows the positions of the selective time in the Q' curve.

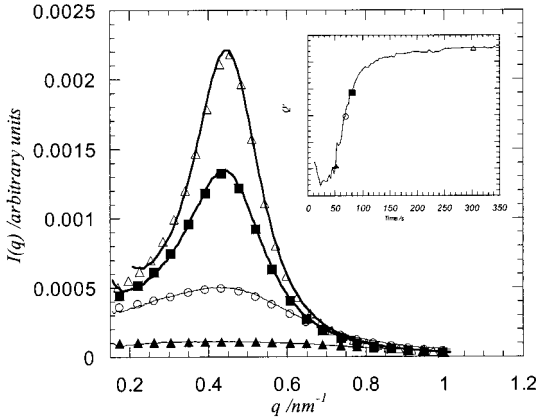

Figure 8. Scattering intensity $I(q)$ at selective time from MDI foam and fitted curves (from eq 6) in various lines as a function of q: (△) 300 s, (■) 84 s, (○) 66 s, (▲) 51 s. The inset shows the positions of the selective time in the Q' curve.

arrested by the vitrification of urea hard domains. Similarly good fits were also obtained for the MDI foam data at four selected times, and these results are shown in Figure 8. This method of analysis is internally consistent, as both the spinodal decomposition kinetics and the Teubner−Strey structure factor are based on a Ginzburg−Landau free energy expansion.

The Teubner−Strey model fitting parameters a_2, c_1, and c_2 for TDI foam and MDI foam are shown in Figure 9. For both foam systems, the coefficient a_2 decreases very rapidly after microphase separation until it is arrested by vitrification. The coefficient c_1 is most closely related to the interfacial tension and is expected to decrease with increasing surfactant concentration.[23] It has been observed that increasing the block copolymer concentration in a ternary polymer blend decreases c_1, since the block copolymer acts as a surfactant.[40] As shown in Figure 9b, c_1 decreases monotonically with time until vitrification occurs and then it levels off. As foaming reactions proceed, the concentration of poly(ether−urea) block copolymer continually increases and effectively acts as a surfactant for the soft and hard segments. The parameter c_2 mainly reflects the large q behavior and is closely related to the structure of the interface. The monotonic increase of c_2 before vitrification indicates a progressive "stiffening" of the interfaces.

Figure 10 shows the values of domain size D plotted as a function of time for MDI foam and TDI foam. The

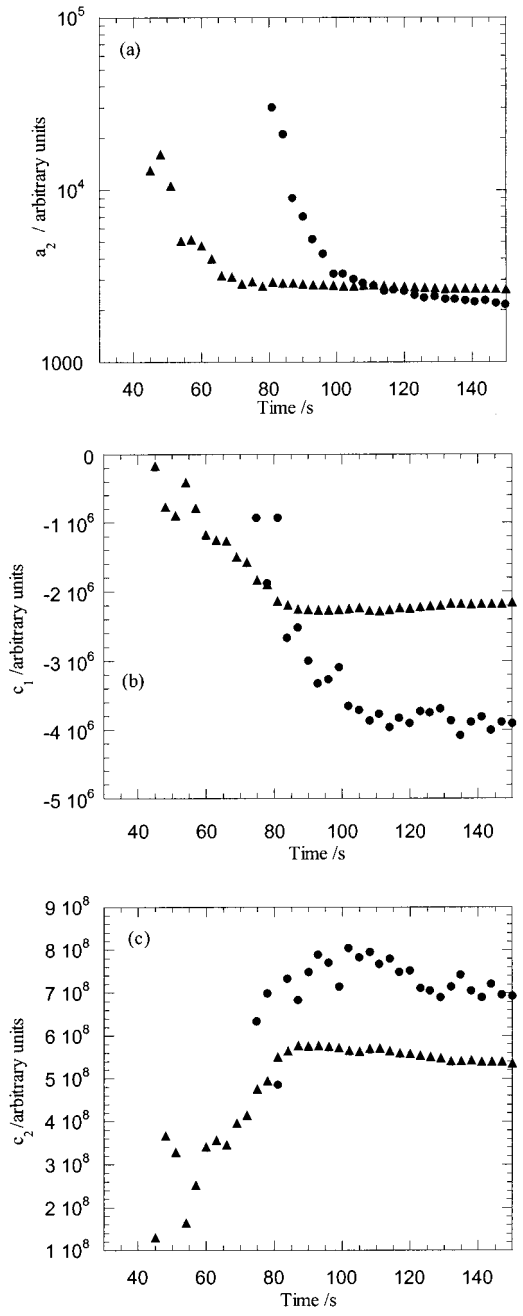

Figure 9. Plots of the Teubner−Strey fitting parameters: (a) a_2, (b) c_1, (c) c_2 as a function of time for MDI foam (▲) and TDI foam (●).

evolution of one-dimensional Bragg spacing (*1-d*) is also shown in Figure 10; using Bragg's law, *1-d* was estimated from the value of q^*, which corresponds to the maximum in the $I(q)q^2$ vs q plot. For both MDI and TDI foam, it was observed that both D and *1-d* continuously increase until the microphase separation is arrested by vitrification. The increase in the interdomain spacing might be due to the increase in the concentration of urea hard segments. The values of D and *1-d* are very close, as expected, because both methods give the same domain size. In Figure 11, ξ/D increases with increasing time, as anticipated from the Teubner−Strey model, due to the increasing concentration of surfactant (i.e., poly(ether−urea) block copolymer). This increase is a characteristic common to surfactant systems. ξ/D is also a measure of domain size polydispersity: the smaller the ratio, the higher the polydispersity.[42]

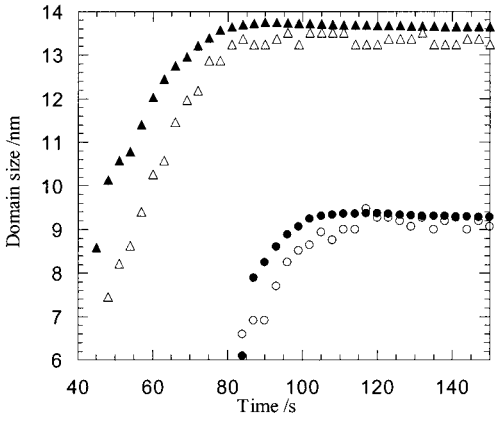

Figure 10. Plots of domain size as a function of time for MDI foam (*D*, ▲; *1-d*, △) and TDI foam (*D*, ●; *1-d*, ○).[26]

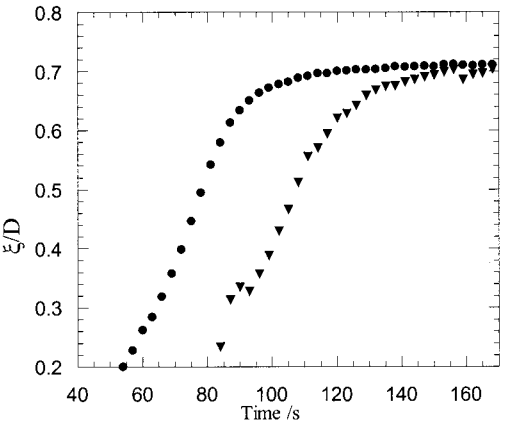

Figure 11. Plots of ξ/D vs time for TDI foam (▲) and MDI foam (●).

For most soft matter systems, there is a delicate balance between entropy and interfacial energy that controls ordering and mixing. The loss of conformational entropy due to the segregation of the blocks at the interfaces is compensated for by the gain in enthalpy as each block is incorporated into the corresponding compatible homopolymer phases so that the overall interfacial tension is decreased. The strength of interaction of the diblock copolymer with the homopolymer phase controls the degree of mixing, and thus it is important to quantify the amphiphilicity of the diblock copolymer.[40,43] During the foaming process, poly(ether−urea) block copolymer forms via urethane groups and can act as a surfactant to stabilize the mixture of immiscible polyether and urea species. Strey et al.[44−46] have classified the differently structured fluids in the disordered phase of the o/w/s system by defining the amphiphilicity factor $f_a \equiv c_1/(4a_2c_2)^{1/2}$, which can be used to extend the Teubner−Strey model to cover all ranges of amphiphilicity. This analysis was subsequently used in the ternary polymer blend systems by Morkved and co-workers.[40] Weak amphiphilicity with $0 < f_a < 1$ results in a "poor" microemulsion. With stronger amphiphilicity, $-1 < f_a < 0$, a well-structured, "good" microemulsion results. One distinguishing characteristic of a good microemulsion is the tendency to create an interface due to a vanishing or negative value of c_1. Further decrease in $f_a < -1$ (i.e., strong amphiphilicity) results in an unstable microemulsion phase with respect to the lamellar phase.[40]

Figure 12 shows the amphiphilicity factors f_a plotted as a function of time for MDI foam and TDI foam. The

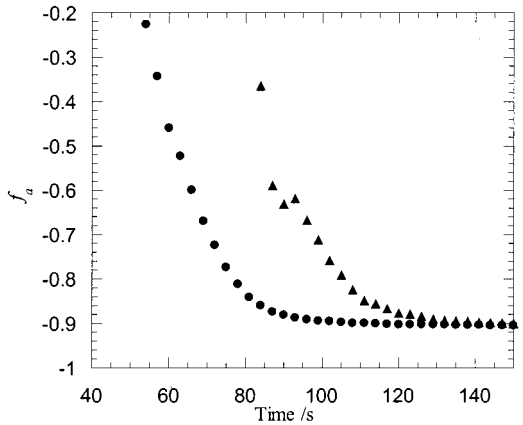

Figure 12. Plots of amphiphilicity factor f_a as a function of reaction time for MDI foam (●) and TDI foam (▲).

value of f_a steadily decreases from nearly 0 to −0.9, indicating that the system is approaching the boundary between a "good" microemulsion and a lamellar structure. Then, after the beginning of vitrification, f_a quickly levels off. This decrease in f_a is due to the continuous formation of block copolymer poly(ether−urea) which reduces the surface tension. Vitrification arrests the structure shortly after the microphase separation occurs, and further increase in the amphiphilicity factor is prevented. If a further increase in the amphiphilicity factor occurred, it would cause the system to transform from a microemulsion structure to a lamellar structure.

The final morphology of MDI foam was studied by AFM, and representative moderate tapping force images are given in Figure 13. The height images are disregarded as the cross sections studied here were microtomed smooth. In a moderate force image, the high phase corresponds to high modulus and low phase to low modulus.[24] Therefore, the lighter phases are richer in polyurea, and the darker phases correspond to the polyol phase in Figure 13. In the low-magnification image, the hard-segment domains fill space relatively uniformly with no gross regions free of hard segment of domains. The hard-segment domains appear to be geometrically anisotropic with dimensions of ca. 10−20 nm wide by 50−100 nm long. The high-magnification image reveals connected hard-segment domains. This is in general agreement with published AFM images[22] which indicated that larger scale structures are aggregates of smaller hard-segment domains.

Transmission electron microscopy (TEM) and SAXS have been used to investigate the morphology of a wide range of lightly cross-linked TDI-based PU foams.[20,47] A single broad SAXS peak similar to those in Figures 2 and 3 was observed, while TEM showed a two-phase irregular bicontinuous structure. A TGDL-based cell dynamics simulation (CDS) has been used by Hamley et al.[41,48] and compared to the morphology observed in the TEM images for PU block copolymers. At the intermediate stage of structure development, CDS shows a microphase-separated morphology with an irregular co-continuous structure with no long-range order, which is similar to the TEM images observed by Neff.[20] However, the late morphology (achieved at equilibrium) in the simulations is a highly developed lamellar structure, with random orientation of lamellae similar to image of triblock copolymers.[24] These observations are consistent with the suggestion that the

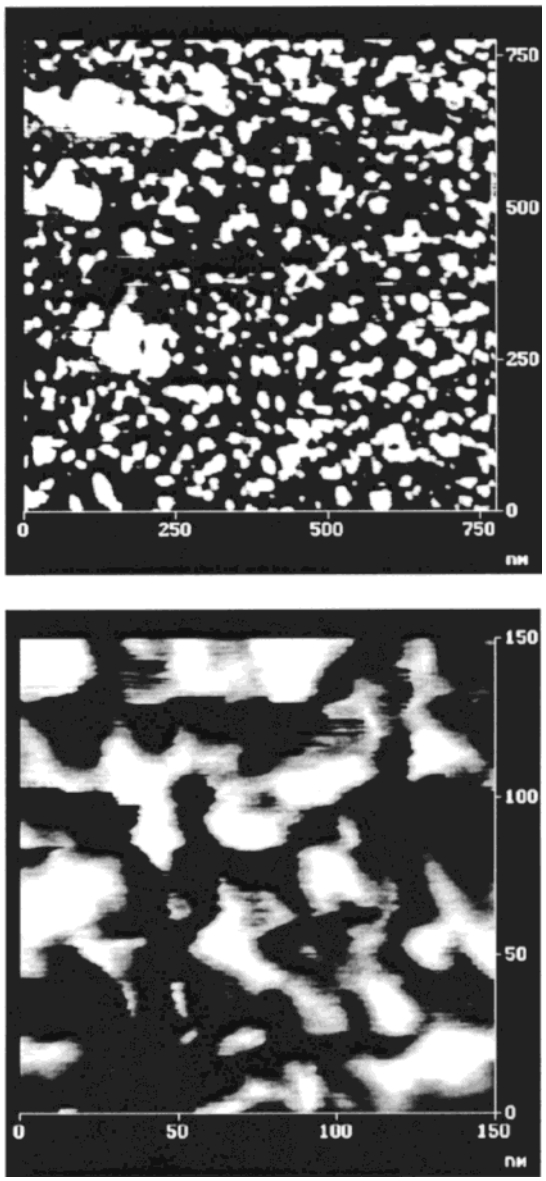

Figure 13. AFM tapping mode phase images at low and high magnification of MDI foam.

vitrification of hard segments prevents the evolution of a structure with well-segregated domains.

Conclusions

For both the TDI and MDI foam systems, the scattering intensity increased exponentially in the early stages of microphase separation. The scattering data were observed to be in good agreement with the predictions of the Cahn−Hilliard model, indicating that microphase separation of urea hard segments proceeds via spinodal decomposition during the formation of flexible polyurethane foam. The SAXS data were analyzed using a Teubner−Strey microemulsion structure factor, which fits the microphase-separated structures well. The bicontinuous morphology was preserved inside the foam because phase separation was quickly arrested by vitrification of urea domains. The RIPS during the foaming process yields a microemulsion structure in a manner similar to the SD of a nonreactive polymer blend under the isoquench depth. The fit also shows that amphiphilicity increases as the reaction proceeds, due to the continuous formation of block copolymer poly(ether−urea). The one-dimensional (1-D) correlation function has been previously applied to polyurethane structures[19] and gives a fair description of the domain spacing, phase volumes, and interfacial thicknesses. Initially there appeared to be a discrepancy between TEM observations and mechanical properties for PU foams, which suggest a bicontinuous morphology, and the interpretation of SAXS patterns, which suggest a lamellar structure. However, this can now be understood in the context of the present results in which a microemulsion is formed at the end of the foaming process, just before the amphiphilicity factor decreases enough for a lamellar structure to result. For both MDI and TDI foam systems, the morphology development sequence is observed to be the same, although the different kinds of polyol and isocyanate are used.

Acknowledgment. This work was financially supported by Air Products & Chemicals, Inc. Ellen Heeley and Anthony Gleeson assisted in the collection of SAXS data. The SAXS cell and control electronics were constructed by Chris Lumley, Mike Carr, and Paul Turner.

References and Notes

(1) Macosko, C. W. *RIM: Fundamentals of Reaction Injection Molding*; Hanser: Munich, 1989.
(2) Ryan, A. J. *Polymer* **1990**, *31*, 707−712.
(3) Yang, W. L. P.; Macosko, C. W. *Makromol. Chem., Macromol. Symp.* **1989**, *25*, 23−44.
(4) Girard-Reydet, E.; Sautereau, H.; Pascault, J. P.; Keates, P.; Navard, P.; Thollet, G.; Vigier, G. *Polymer* **1998**, *39*, 2269−2279.
(5) Yamanaka, K.; Takagi, Y.; Inoue, T. *Polymer* **1989**, *30*, 1839−1884.
(6) Kim, B. S.; Chiba, T.; Inoue, T. *Polymer* **1995**, *36*, 43−47.
(7) Pearson, R. A. In *Advances in Chemistry Series 233*; Riew, C. K.; Kinloch, A. J., Eds.; American Chemical Society: Washington, DC; p 405.
(8) Elwell, M. J.; Ryan, A. J.; Grunbauer, H. J. M.; VanLieshout, H. C. *Macromolecules* **1996**, *29*, 2960−2968.
(9) Artavia, L. D. University of Minesota, 1991.
(10) Artavia, L. D.; Macosko, C. W. In *Proceedings of the 33rd SPI Annual Technical & Marketing Conference*; Technomic Publishing Co.: Lancaster, PA, 1990.
(11) Priester, R. D.; McCluskey, J. V.; O'Neill, R. E.; Turner, R. B.; Harthcock, M. A.; Davis, B. L. *J. Cell. Plast.* **1990**, *26*, 346−365.
(12) McClusky, J. V.; Priester, R. D.; Oneill, R. E.; Willkomm, W. R.; Heaney, M. D.; Capel, M. A. *J. Cell. Plast.* **1994**, *30*, 338−360.
(13) Elwell, M. J.; Ryan, A. J.; Grunbauer, H. J. M.; VanLieshout, H. C. *Polymer* **1996**, *37*, 1353−1361.
(14) Neff, R.; Macosko, C. W. In *35th Annual Polyurethane Technical/Marketing Conference*, 1994.
(15) Mora, E.; Artavia, L. D.; Macosko, C. W. *J. Rheol.* **1991**, *35*, 921−940.
(16) McCluskey, J. V.; Oneill, R. E.; Priester, R. D.; Ramsey, W. A. *J. Cell. Plast.* **1994**, *30*, 224−241.
(17) Elwell, M. J.; Mortimer, S.; Ryan, A. J. *Macromolecules* **1994**, *27*, 5428−5439.
(18) Cooper, S. L.; Li, C. *Polymer* **1990**, *31*, 3.
(19) Armistead, J. P.; Wilkes, G. L.; Turner, R. B. *J. Appl. Polym. Sci.* **1988**, *35*, 601−629.
(20) Neff, R.; Adedeji, A.; Macosko, C. W.; Ryan, A. J. *J. Polym. Sci., Part B: Polym. Phys.* **1998**, *36*, 573−581.
(21) Mclean, R. S.; Sauer, B. B. *Macromolecules* **1997**, *30*, 8314−8317.
(22) Garrett, J. T.; Siedlecki, C. A.; Runt, J. *Macromolecules* **2000**, *34*, 7066−7070.
(23) Teubner, M.; Strey, R. *J. Chem. Phys.* **1987**, *87*, 3195.
(24) McLean, R. S.; Sauer, B. B. *Macromolecules* **1997**, *30*, 8314−8317.
(25) Glatter, O., Kratky, O., Eds.; *Small-Angle X-ray Scattering*; Academic Press: London, 1983.
(26) Li, W. In *Chemistry*; University of Sheffield, 2001.
(27) Cahn, J. W.; Hilliard, J. E. *J. Chem. Phys.* **1958**, *28*, 258.

(28) Hashimoto, T. *Macromolecules* **1987**, *20*, 465.
(29) Connell, J. G.; Richards, R. W.; Rennie, A. R. *Polymer* **1991**, *32*, 2033.
(30) Mallamace, F.; Micali, N.; Trusso, S. *J. Phys.: Condens. Matter* **1996**, *8*, A81.
(31) Binder, K. In *Materials Science and Technology: A Comprehensive Treatment*; Cahn, R. W., Haasen, P., Kramer, E. J., Eds.; VCH Publishers: Weihheim, 1991; p 405.
(32) Olabisi, O.; Robeson, L. M.; Shaw, M. T. *Polymer−Polymer Miscibility*; Academic Press: New York, 1977.
(33) Huston, E. L.; Cahn, J. W.; Hilliard, J. E. *Acta Metall.* **1966**, *14*, 1053.
(34) Ohnaga, T.; Chen, W. J.; Inoue, T. *Polymer* **1994**, *35*, 3774−3781.
(35) Lee, J. H.; Jeon, H. S.; Balsara, N. P.; Newstein, M. C. *J. Chem. Phys.* **1998**, *105*, 5173−5176.
(36) Jackson, C. L.; Sung, L.; Han, C. C. *Polym. Eng. Sci.* **1997**, *37*, 1.
(37) Kawakatsu, K. *J. Chem. Phys.* **1993**, *99*, 8200.
(38) Komura, S.; Seto, H.; Takeda, T.; Nagao, M.; Ito, Y. J.; Imai, M. *J. Chem. Phys.* **1996**, *105*, 3264−3277.
(39) Hillmyer, M. A.; Maurer, W. W.; Lodge, T. P.; Bates, F. S.; Almdal, K. *J. Phys. Chem. B* **1999**, *103*, 4814−4824.
(40) Morkved, T. L.; Stepanek, P.; Krishnan, K.; Bates, F. S.; Lodge, T. P. *J. Chem. Phys.* **2001**, *114*, 7247−7259.
(41) Hamley, I. W.; Stanford, J. L.; Wilkinson, A. N.; Elwell, M. J.; Ryan, A. J. *Polymer* **2000**, *41*, 2569−2576.
(42) Chen, S.-H.; Chang, S. L.; Strey, R. *Prog. Colloid Polym. Sci.* **1990**, *81*, 30.
(43) Gelbart, W. M., Ben-Shaul, A., Rous, D., Eds.; *Micelles, Membranes, Microemulsions, and Monolayers*; Springer: New York, 1994.
(44) Koehler, R. D.; Schubert, K. V.; Strey, R.; Kaler, E. W. *J. Chem. Phys.* **1994**, *101*, 10843−10849.
(45) Schubert, K. V.; Strey, R. *J. Chem. Phys.* **1991**, *95*, 8532−8545.
(46) Schubert, K. V.; Strey, R.; Kline, S. R.; Kaler, E. W. *J. Chem. Phys.* **1994**, *101*, 5343−5355.
(47) Dounis, D. V.; Wilkes, G. L. *J. Appl. Polym. Sci.* **1997**, *65*, 525−537.
(48) Hamley, I. W. *Macromol. Theory Simul.* **2000**, *9*, 363−380.

MA020035E